# Electron-phonon interactions in MoS2 probed with ultrafast two-dimensional visible/far-infrared spectroscopy

Xunmin Guo, Hailong Chen, Xiewen Wen, and Junrong Zheng

---

**Articles you may be interested in**

Quantum confinement effects across two-dimensional planes in MoS2 quantum dots
Appl. Phys. Lett. **106**, 233113 (2015); 10.1063/1.4922551

Charge carrier dynamics in bulk MoS2 crystal studied by transient absorption microscopy
J. Appl. Phys. **113**, 133702 (2013); 10.1063/1.4799110

Two-dimensional electron gases: Theory of ultrafast dynamics of electron-phonon interactions in graphene, surfaces, and quantum wells
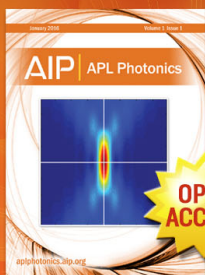J. Appl. Phys. **105**, 122409 (2009); 10.1063/1.3117236

Spectroscopy of the electron–phonon interaction in the layered two-dimensional dichalcogenide 1T –VSe 2
Low Temp. Phys. **27**, 56 (2001); 10.1063/1.1344144

Ultrafast dynamics of holes in GaAs probed by two-color femtosecond spectroscopy
Appl. Phys. Lett. **73**, 64 (1998); 10.1063/1.121724

---

# Electron-phonon interactions in MoS$_2$ probed with ultrafast two-dimensional visible/far-infrared spectroscopy

Xunmin Guo,[a)] Hailong Chen,[a)] Xiewen Wen, and Junrong Zheng[b)]

*Department of Chemistry, Rice University, 6100 Main Street, Houston, Texas 77005-1892, USA*

An ultrafast two-dimensional visible/far-IR spectroscopy based on the IR/THz air biased coherent detection method and scanning the excitation frequencies is developed. The method allows the responses in the far-IR region caused by various electronic excitations in molecular or material systems to be observed in real time. Using the technique, the relaxation dynamics of the photo-excited carriers and electron/phonon coupling in bulk MoS$_2$ are investigated. It is found that the photo-generation of excited carriers occurs within two hundred fs and the relaxation of the carriers is tens of ps. The electron-phonon coupling between the excitations of electrons and the phonon mode E$_{1u}$ of MoS$_2$ is also directly observed. The electron excitation shifts the frequency of the phonon mode 9 cm$^{-1}$ higher, resulting in an absorption peak at 391 cm$^{-1}$ and a bleaching peak at 382 cm$^{-1}$. The frequency shift diminishes with the relaxation of the carriers. © *2015 AIP Publishing LLC.* [http://dx.doi.org/10.1063/1.4921573]

## I. INTRODUCTION

Electron-phonon (lattice vibrations) interactions are ubiquitous and essential in many physical and chemical processes. For example, the coupling between electrons and phonons is suggested to be responsible for conventional superconductivity.[1–5] Finding a way to directly observe the electron-phonon coupling in high-transition-temperature superconductors is of great importance for the study and the improvement of high-temperature superconductors.[6] In optoelectronic devices, the interaction of electrons with phonons is critical for the heat generation and dissipation,[7,8] which determines the device temperature and the power efficiency. In two-dimensional (2D) materials, such as layered transition metal dichalcogenides (TMDs) (e.g., MoS$_2$ and WS$_2$),[9] phonons usually have some distinct vibrational frequencies in the far-infrared (far-IR) region, between about 100 cm$^{-1}$ and 500 cm$^{-1}$. When electrons in these materials are excited, the electronic energy will be converted to the excitations of these vibrational modes (phonons), besides the emission of photons through fluorescence (or phosphorescence). The excitations of these phonon modes dissipate within the 2D sheet and through layers and to the environment, and raise the temperature. The energy dissipation pathways and the thermal properties of 2D materials and the hetero-structures based on them are determined by the generation, dissipation, and transfer dynamics of these phonon excitations. To investigate these dynamics, a spectroscopy with tunable excitation wavelengths and broadband detection frequency which can cover the entire far-IR region is needed.

Some traditional methods, such as the optical pump terahertz (THz) probe spectroscopy,[10–12] usually employ the electro-optic effect of ZnTe[13] or photoconductive emitter[14] to generate THz pulse, of which the detection frequencies are limited to be below 2-3 THz ($<$100 cm$^{-1}$) unless a very short pulse ($\leq$15 fs) is used. As a result, these methods are mainly limited for the investigation of the carrier dynamics. The electron-phonon interactions with phonons at frequencies $>$100 cm$^{-1}$ (e.g., optical phonons in TMDs) cannot be studied by the methods. Although the THz pulse with higher frequencies can be generated by some groups,[15,16] a pump source with ultra-short pulse duration (10-15 fs) is needed. Traditional femtosecond stimulated Raman spectroscopy, which consists of a femtosecond visible pump, a narrow bandwidth picosecond Raman pump, and a femtosecond continuum probe,[17–21] have been applied to obtain vibrational spectra of transient electronic states. However, it is still very challenging for the method to collect signals at lower frequencies, e.g., tens of cm$^{-1}$, and it is also very difficult to directly monitor the dynamics of charge carriers. In addition, it was recently shown that, limited by the Fourier uncertainty, only some of the probe modes contribute to the femtosecond stimulated Raman signal.[22,23]

In this work, we will introduce an ultrafast two-dimensional visible/far-IR spectroscopy that can directly monitor the electron/phonon couplings. In the method, the optical excitation wavelength is tunable and the detection frequency is a broadband which covers the entire far-IR region. Using this technique, the carrier dynamics and electron-phonon interactions of a bulk MoS$_2$ sample with the excitation of electrons from the valence band to the conduction band are investigated.

## II. EXPERIMENTS

The optical setup of the ultrafast two-dimensional visible/far-IR spectroscopy is based on the scanning of

---

a)X. Guo and H. Chen contributed equally to this work.
b)Author to whom correspondence should be addressed. Electronic mail: junrong@rice.edu
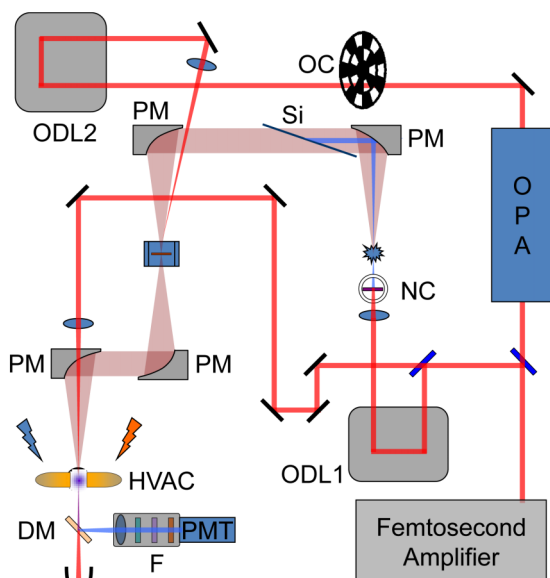
**142**, 212447-1

FIG. 1. Illustration of the optical setup. OPA: optical parametric amplifier; OC: optical chopper; ODL1&ODL2: optical delay line; NC: nonlinear crystal BBO; PM: parabolic mirror; Si: silicon wafer; HVAC: high voltage AC electrodes; DM: dichroic mirror; F: filters; PMT: photomultiplier tube.

visible excitation frequencies and the detection of far-IR/THz frequencies by the air biased coherent detection method (THz-ABCD).[24–26] As displayed in Fig. 1, the output of a femtosecond amplifier laser system (800 nm central wavelength, 1.6 mJ energy, 50 fs duration, 1 kHz repetition rate, Uptek Solutions, Inc.) is split into three beams. The major portion (0.9 mJ), after traveling through an optical delay line, is frequency-doubled by a nonlinear crystal (0.2 mm thick BBO). The mixture of the residual fundamental beam and the generated 400 nm light is then focused into the ambient air, producing intense air plasma. A broadband THz radiation covering a very broadband far-IR region up to midIR is generated from the air plasma through a process similar to four wave rectification.[27–32] After removing the residual optical beams with a silica wafer at the Brewster angle, the emitted far-IR pulse is then collected and focused into the sample with the beam waist estimated to be smaller than 1 mm at the frequency larger than 200 cm$^{-1}$.

For the coherent detection of far-IR electric field, the second portion of fundamental laser source (0.1 mJ) is introduced as the readout beam to mix with the transmitted far-IR beam from sample. Both beams are then focused into air at the same focal point, where a high voltage bias field (10 kV/cm, generated by Bi3KV HV Mod, Uptek Solutions, Inc.) is applied. As a result, both the far-IR-electric-field-induced second harmonic $E_{2\omega}^{THz}$ (proportional to the amplitude of far-IR electric field) and the bias-induced second harmonic $E_{2\omega}^{HV}$ are simultaneously generated through the medium of air molecules. Cleaned with a dichroic mirror and a combination of short-pass and band-pass filters, the superposition of the second harmonic generations $I_{2\omega} \propto (E_{2\omega}^{THz} + E_{2\omega}^{HV})^2$ is detected by a photomultiplier tube (PMT). By modulating the high voltage bias field at the sub-harmonic repetition frequency of amplifier laser system (500 Hz) and referring the lock-in amplifier to this frequency, the cross term of the superposition $I_{2\omega}$ which is proportional to

the amplitude of the far-IR electric field is isolated from the DC background. The time domain spectrum of far-IR wave $E_0(t)$ is obtained by scanning the optical delay line (ODL1) and recording the far-IR electric field amplitude as a function of delay time $t$.[24,26,33–35]

The third portion of the fundamental laser source (0.6 mJ) is used to drive an optical parametric amplifier (OPA) to produce a widely tunable visible or near IR light source. After attenuated to a few $\mu$J and delayed by $T_W$ through a 2nd optical delay line (ODL2), the visible excitation beam is focused on the sample, spatially overlapping with the far-IR beam spot with a slightly larger beam waist (>1 mm). Therefore, the incident excitation energy density is smaller than 500 $\mu$J/cm$^2$. To extract the visible excitation induced absorption change of the sample, an optical chopper with a blade of 7/5 slots is placed on the excitation beam path, modulating the excitation beam by the inner ring (5 slots) and synchronizing the outer ring (7 slots) with the detection modulation frequency (500 Hz). Thus, the modulation frequency of the excitation beam is $500 * 5/7 = 357.1$ Hz. Since the detection beam is modulated at 500 Hz by HVAC, the band-pass extracting response signal around the sum frequency of excitation and the detection modulation frequency (500 + 357.1 = 857.1 Hz) can exclusively provide the detected intensity changes induced only by the excitation beam. Therefore, another lock-in amplifier referenced at that sum frequency (857.1 Hz) is used to acquire the excitation-induced amplitude change of the far-IR electric field $\Delta E(t)$. Simultaneously, the excitation-present amplitude of far-IR electric field $E(t)$ is collected by the first lock-in amplifier referenced at the detection modulation frequency (500 Hz). By subtracting $\Delta E(t)$ from $E(t)$, the excitation-absent far-IR electric field amplitude $E_0(t)$ is obtained.

With this scheme, the signal to noise ratio (SNR) of the measured $\Delta E(t)$ can be achieved up to 100:1. The instrument response function (IRF) of the visible/far-infrared spectroscopy is about 150 fs, which was estimated from the excitation-induced free carriers signal in silicon. All relevant field components (bias electric field, fundamental beam, and the excitation beam) are parallelly polarized to each other. Therefore, only the parallel response of visible/far-IR transient absorbance will be measured.

It is worthwhile to emphasize that, to detect the chirp-free response of transient absorption, the relative time delay between the fundamental readout beam and the pump beam is conserved when scanning $t$ at a specific $T_W$.[12,15,36–39]

Data are obtained as a function of three variables: the excitation wavelength from OPA ($\lambda_E$), the variable time delay $t$ between the far-IR beam and the fundamental readout beam which can be further converted to the detection frequency by Fourier transform, and the variable waiting time $T_W$ between the far-IR beam and the excitation beam. The absorbance change at a certain excitation-detection delay is plotted as a function of excitation wavelength and detection frequency. For a given excitation wavelength, the waiting time dependent change of absorption spectra reflects the excitation-induced ultrafast broadband response in the far-IR region. Slices of these spectra at any specific detection frequencies display dynamic evolution of transient species involved.

All the experiments are performed at room temperature except the temperature dependent measurements of the static spectra. Molybdenum disulfide ($MoS_2$) multi-layer single crystal is purchased from 2D Semiconductors, Inc., and used as received. Sample flakes are prepared and dried by smearing acetone mull containing $MoS_2$ chip on the polyimide thin film. All the measurements are performed with the far-IR light perpendicular to the crystallographic c-axis of bulk $MoS_2$. Control experiments on the polyimide thin film are conducted. The results demonstrate much less steady-state absorption in both excitation wavelength range (550-800 nm) and detection frequency range (50-420 $cm^{-1}$) of the film, compared to the $MoS_2$ crystal. Besides, the polyimide thin film shows no contribution to the excitation-induced transient absorption measurements.

## III. RESULTS AND DISCUSSION

Fig. 2(a) displays the respective time domain spectra $E_0(t)$ and $E_0'(t)$ of the bulk $MoS_2$ sample on polyimide and the polyimide substrate. After applying Fourier transform, the power spectra $|E_0(\omega)|^2$ and $|E_0'(\omega)|^2$ are obtained, displayed in the inset of Fig. 2(b). The absorption spectrum of the pure bulk $MoS_2$ sample in the far-IR region is obtained from the measurements, calculated with the expression $-\log(|E_0(\omega)|^2/|E_0'(\omega)|^2)$. As displayed in Fig. 2(b), a sharp peak around 382 $cm^{-1}$ (with an uncertainty of 2–3 $cm^{-1}$) clearly shows up in the absorption spectrum of the bulk $MoS_2$ in the far-IR region. This peak is assigned to the IR active in-plane phonon mode $E_{1u}$ of the bulk $MoS_2$, according to previous experimental and calculated results.[40–44]

To investigate the optoelectronic response and the electron-phonon coupling in bulk $MoS_2$, we first use the 800 nm (1.55 eV) laser pulse to excite the electrons in $MoS_2$ from the valence band to the conduction band, and monitor the transition absorption dynamics in the far-IR region. In the experiments, the increase of the lattice temperature induced by the pump excitation is very small (on the order of ~0.1 K). The calculation is based on the pump power (~500 $\mu J/cm^2$) and the heat capacity of the bulk $MoS_2$ (~63.7 J/(mol K)).

Besides, the experiments were also conducted at a much lower excitation power (~35 $\mu J/cm^2$), and all the results are unchanged within experimental uncertainty. The detailed calculation of the temperature and the experimental results at lower excitation power are provided in supplementary material.[51] As a result, the laser simply perturbs the electronic state of the bulk $MoS_2$ rather than photo-inducing a phase transition.[45]

Fig. 3(a) and the inset display the excitation-induced amplitude change of transmitted far-IR electric field $\Delta E(t)$ (black line), the excitation-present amplitude of far-IR electric field $E(t)$ (red line), and the excitation-absent far-IR electric field amplitude $E_0(t)$ (blue line). Both black and red lines are recorded at the same excitation wavelength of 800 nm at the waiting time $T_W = 2$ ps. The results clearly show that the optical excitation induces a drop of the far-IR electric field amplitude. The frequency domain spectra Fourier transformed from Fig. 3(a) are displayed in Fig. 3(b). The negative absorption change of bulk $MoS_2$ (down panel in Fig. 3(b)) can be written in terms of time domain spectra of far-IR fields by the following equation:

$$-\Delta OD(\omega) = \log(\frac{I(\omega)}{I_0(\omega)}) = \log(\frac{|F(E(t))|^2}{|F(E_0(t))|^2})$$

$$= \log(\frac{|F(E(t))|^2}{|F(E(t) - \Delta E(t))|^2}), \quad (1)$$

where $F(f(t))$ indicates the Fourier transform of $f(t)$.

It can be seen that the optical excitation induces an absorption increase (negative peak) in most of the detection frequencies. At frequencies around 382 $cm^{-1}$, a sharp positive peak and a negative peak appear, with center frequencies at 382 $cm^{-1}$ and 391 $cm^{-1}$, respectively. The central frequencies of the two peaks are obtained by fitting two peaks with the superposition of two Gaussian line shapes (see supplementary material[51]). The origins of these two peaks will be discussed in the following.

By tuning the time delay $T_W$, the waiting time dependent excitation-induced negative absorption change are obtained (Fig. 4(a)). At waiting times $T_W > 0$, a broadband featureless negative signal dominates each of the spectra (Fig. 4(b)),
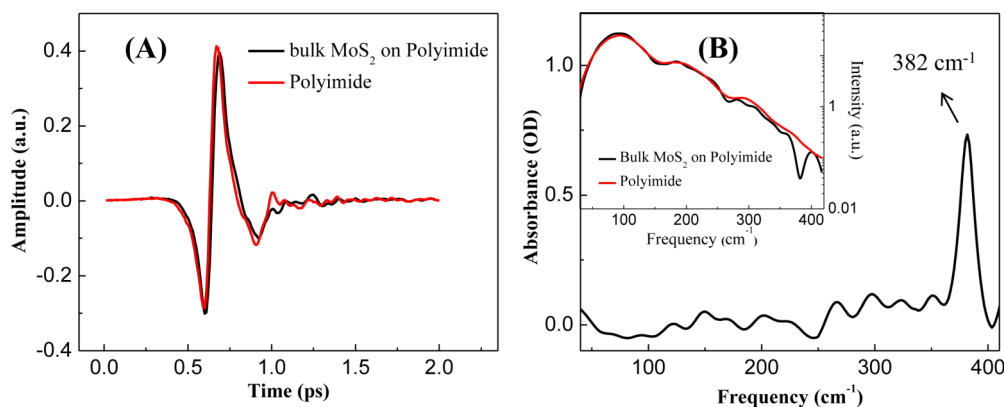


FIG. 2. (a) Time domain spectra $E_0(t)$ and $E_0'(t)$ of the bulk $MoS_2$ sample on polyimide (black line) and the polyimide substrate (red line), respectively. (b) The absorption spectrum of the pure bulk $MoS_2$ sample in the far-IR region. The peak at 382 $cm^{-1}$ is the IR active in-plane phonon mode $E_{1u}$ of the bulk $MoS_2$. Inset: the frequency domain power spectra of the bulk $MoS_2$ sample on polyimide (black line) and the polyimide substrate (red line), obtained from the Fourier transform of the time domain spectra in (a).
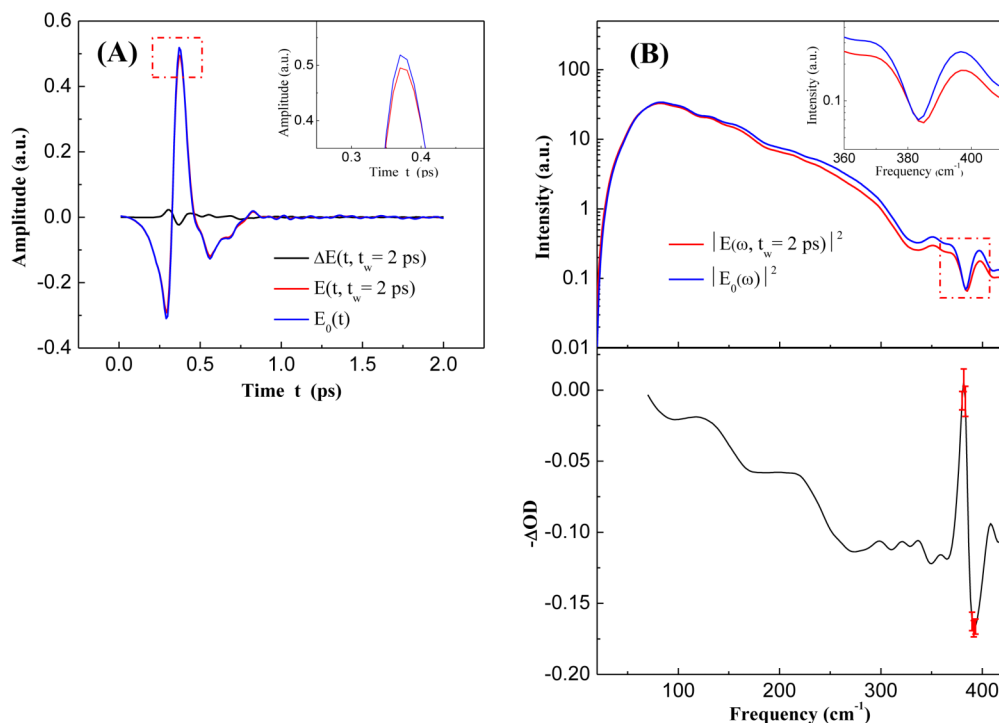
FIG. 3. The time and frequency domain steady and transient spectra of bulk MoS$_2$. (a) The measured excitation-induced amplitude change of transmitted far-IR electric field $\Delta E(t)$ (black line), the measured excitation-present amplitude of far-IR electric field $E(t)$ (red line), and the excitation-absent far-IR electric field amplitude $E_0(t)$ (calculated from $E(t) - \Delta E(t)$, blue line). Both black and red lines are recorded at the excitation wavelength of 800 nm (centered) and the waiting time $T_W = 2$ ps. Inset: a zoomed-in view of the electric field peaks (dashed square). (b) Upper panel: the calculated power spectra of far-IR transmitted intensity with excitation-present (red, $|E(\omega)|^2$) and excitation-absent (blue, $|E_0(\omega)|^2$). Inset: a zoomed-in view around the phonon resonant peak E$_{1u}$ (dashed square). Bottom panel: the calculated excitation-induced negative absorption change of MoS$_2$ at a waiting time $T_W = 2$ ps with error bars for the peaks, which is calculated according to Eq. (1).
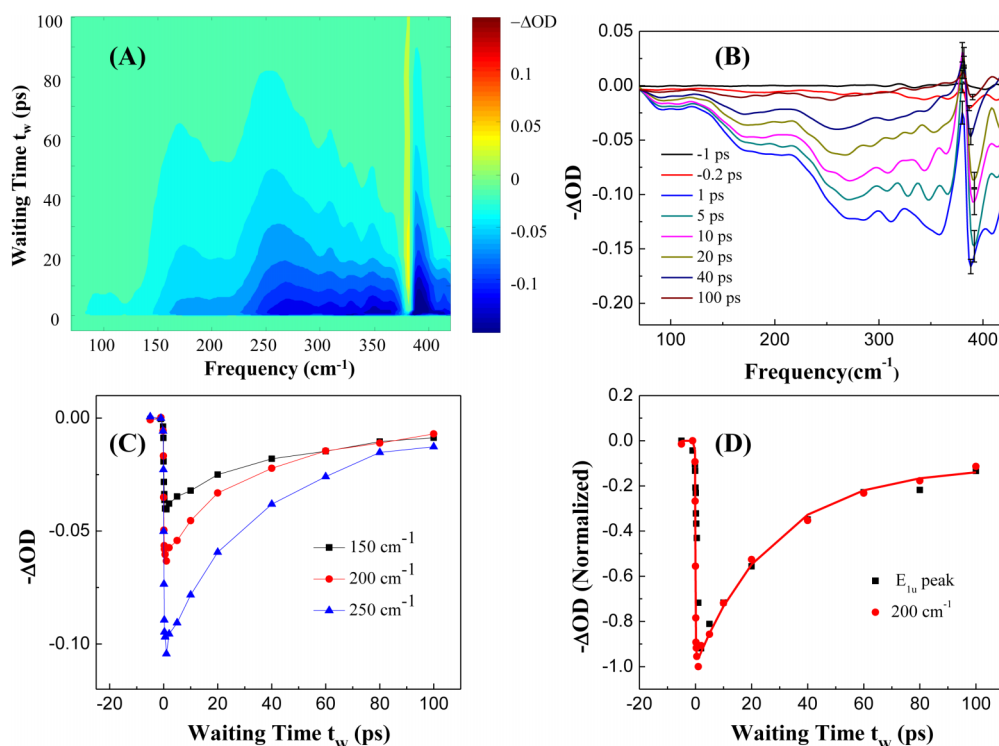


FIG. 4. (a) Waiting time dependent excitation-induced negative absorption change of the bulk MoS$_2$. The wavelength of the exciting pulse is centered at 800 nm. (b) Excitation-induced negative absorption change of the bulk MoS$_2$ at different waiting times. (c) Temporal evolution of the excitation-induced negative absorption change at three different frequencies. (d) Comparing the normalized waiting time dependent signal from the phonon mode E$_{1u}$ (black dots) with that from photo-excited carriers (measured at 200 cm$^{-1}$, red dots). The red curve is the double exponential fit for the detected signal at 200 cm$^{-1}$ with the consideration of IRF (150 fs). The fitting result shows a rising constant of $160 \pm 20$ fs and a decay constant of $28 \pm 3$ ps.

which indicates the transient increase of absorbed far-IR light after optical excitation. Fig. 4(c) displays the temporal evolution of this featureless signal at different frequencies. After excitation with the 800 nm light, the intensities of signals increase rapidly within about two hundred fs, and then decay with almost the same rate at different detection frequencies. According to the literature, the optical excitation enhanced absorption signal at these frequencies can be attributed to the absorption of photo-generated free carriers in bulk $MoS_2$, and the conductivity spectra of which can be roughly described by the Drude formula.[46] However, an opposite slope of the transient spectrum was observed here, i.e., decreasing absorption with lowering frequencies. One likely reason is that, the spot size of the excitation beam is not large enough to completely cover the entire detection beam, especially for light at lower frequencies, and therefore leading to a decreasing signal. Detailed discussions about the normalization are provided in the supplementary material. However, because experimentally we do not know the exact spatial profile of the overlap of excitation/probe beams, we cannot exclude other possibilities that may also cause such an observation. For example, it is also possible that the localization of carrier rather than a free carrier response contributes to the signal.

Fitting the waiting time dependent signal of the photo-excited carrier with the convolution of a double exponential function and the IRF, the generation and recombination time constants of the carrier are obtained, which are $160 \pm 20$ fs and $28 \pm 3$ ps, respectively (Fig. 4(d)). The former is close to the IRF (150 fs), indicating a very fast generation process. Our experimental results (in supplementary material) on samples of various sizes and shapes strongly suggest that the recombination rate of the photo-excited carrier can be much longer than tens of ps, dependent on the sizes and shapes of $MoS_2$ chips, while the generation rate remains constant. The quantitative connection between the $MoS_2$ size and shape and the measured recombination rates will be subject to future studies.

In Figs. 4(a) and 4(b), among the featureless broadband absorption, a sharp positive peak (transient decrease of the absorption) at around 382 cm$^{-1}$ and a sharp negative peak (transient enhancement of the absorption) at around 391 cm$^{-1}$ appear. The frequencies are close to that of the absorption peak of the phonon mode $E_{1u}$ (Fig. 2(b)). Therefore, it is very conceivable that the appearances of the positive peak and the negative peak are related to the phonon mode $E_{1u}$. The difference of the signal intensity between the negative peak and the positive peak is plotted in Fig. 4(d). (That the difference rather than the individual intensity is plotted is to suppress the effect of background.) Similar to the photo-excited carrier signals, after the excitation, the intensities of the signal from the phonon mode increase rapidly within a couple of hundreds fs and then decay relatively slowly at the time scale of tens of ps.

According to the principles of transient vibrational signal generation,[47] the appearances of peaks at around 380–390 cm$^{-1}$ may arise from three possible origins: (1) the energy transfer from the electronic state to the phonon state, (2) the laser heating effect, and (3) the electron-phonon coupling. Let us consider the 1st possibility. If the signals

are dominated by the energy transfer from the electronic state to the phonon mode $E_{1u}$, the positive peak at 382 cm$^{-1}$ and the negative peak at 391 cm$^{-1}$ should represent the 0-1 (from the ground state to the 1st excited state) transition and 1-2 (from the 1st to the 2nd excited state) transition of the mode $E_{1u}$, respectively. However, the frequency of the 1-2 transition is usually lower than that of the 0-1 transition because of vibrational anharmonicities,[47] which is opposite to the experimental results (see Fig. 4(b)). Therefore, based on the analysis of the peak frequencies, we conclude that it is very unlikely that the two peaks are generated because of the direct electron/phonon energy transfer.

Laser heating can shift the absorption frequency of a phonon (or vibration) mode.[48] It is worth noting that the phonon mode $E_{1u}$ is also a heat carrier in the $MoS_2$ crystal. In principle, the heat generated by the absorption of energy from the excitation laser can dissipate to mode $E_{1u}$ and/or other phonon modes. The 1st situation (heat directly to mode $E_{1u}$) is identical to the energy transfer from the electronic state to the phonon state as discussed above, which is already excluded. In the latter situation, the frequency of the phonon mode $E_{1u}$ can be affected by the excitation of other phonon modes of which the frequencies are usually lower than that of $E_{1u}$. However, from the literature[49] and experimental results presented in Fig. 4(c), it is found that it takes about tens of ps for the hot carriers to relax their energy until they reach thermal equilibrium with the lattice in bulk $MoS_2$ crystal. If the appearances of peaks at 380–390 cm$^{-1}$ were caused by the hot carrier relaxation, we would have observed a gradual increase of their intensities with a time constant of tens of ps. However, experimental results in Fig. 4(d) show a very rapid increase within about 200 hundred fs, different from this prediction. Therefore, the peaks at 380–390 cm$^{-1}$ should not be caused by the laser heating. This conclusion is further confirmed by measuring the temperature dependent absorption change of the bulk $MoS_2$, as shown in Fig. 5. At a higher temperature, the frequency of the peak is lower, opposite to the new absorption peak in Fig. 4(b) that appears at a higher frequency. The temperature dependent measurements indicate
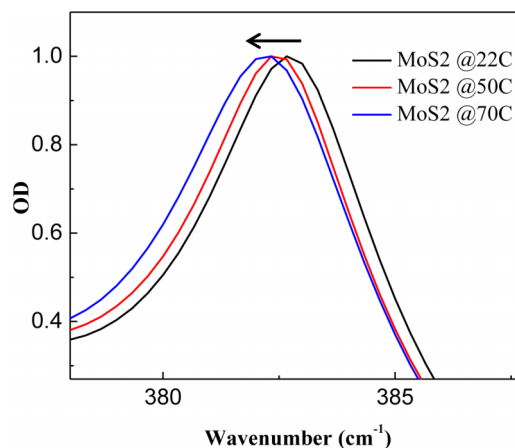


FIG. 5. The frequency change of the phonon mode $E_{1u}$ at different temperature: 22 °C, 50 °C, and 70 °C. The arrow denotes the increasing direction of the temperature, which indicates the frequency of the phonon mode becomes lower at a higher temperature.

**(A)**



Rephasing    $k_e = -k_1 + k_2 + k_3$     Nonrephasing    $k_n = k_1 - k_2 + k_3$

**(B)**

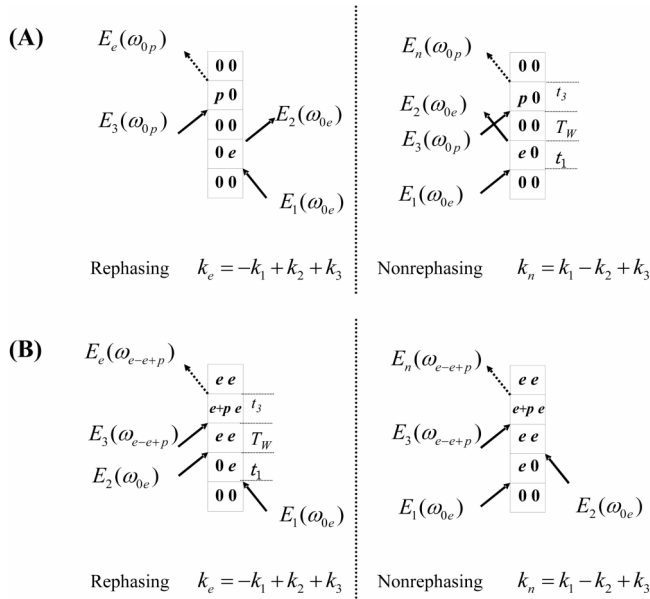Rephasing    $k_e = -k_1 + k_2 + k_3$     Nonrephasing    $k_n = k_1 - k_2 + k_3$

FIG. 6. The rephasing and nonrephasing Feynman diagrams contributing to the observed electron-phonon coupling signals: (a) for the positive peak at 382 cm$^{-1}$ and (b) for the negative peak at 391 cm$^{-1}$. 0, $e$, $p$, and $e+p$ represent the ground state, the electronic excited state, the 1st excited state of phonon mode $E_{1u}$, and the combinational band of electronic excited state and the excited state of phonon mode of bulk MoS$_2$.

indicates that the excitation of the electrons from the valence band to the conduction band shifts the absorption of the optical phonon $E_{1u}$ from 382 cm$^{-1}$ to a higher frequency, resulting in a new absorption at 391 cm$^{-1}$ and a bleaching at 382 cm$^{-1}$. The signal generations can be understood in terms of the Feynman diagrams in Fig. 6. After the laser excitation (the first two interactions $E_1$&$E_2$), the electrons from the valence band are excited to the conduction band, forming photo-excited carriers. The electronic excitation leads to an almost simultaneous frequency shift of mode $E_{1u}$ (in the diagrams, the frequency shift is the difference between $\omega_{e-e+p}$ and $\omega_{0p}$). In the experiments, the frequencies of mode $E_{1u}$ are detected by $E_3$&$E_s$ ($E_s = E_e$ and $E_n$) during the period ($T_w$) after the electrons are excited. At the very first few hundred fs, the amount of photo-excited carriers increases, and therefore the signals of the frequency shift of $E_{1u}$ also increase. With the increase of the delay time, the photo-excited carriers gradually relax, and the signals of the frequency shift gradually decrease. In principle, the relaxation of photo-excited carriers must have some probability to produce the excitation of mode $E_{1u}$. However, we do not clearly observe such a vibrational excitation from Figs. 4(a) and 4(b). One likely reason is that the electron/phonon coupling signal is much larger than the vibrational excitation signal which is partially diminished by the very short lifetime of mode $E_{1u}$ (estimated to be only 1–2 ps).[46,50]

The coupling induced frequency shift of the phonon mode may arise from a Stark shift of the phonon mode by the presence of excitation-induced charge carriers, or because the presence of excitation-induced charges affects the frequency dependent dielectric constant of the sample that in turn shifts the phonon frequency. The detailed coupling mechanism needs to be confirmed by further experiments and calculations. One feasible way is to collect the absorption change of the MoS$_2$ sample with the excitation of the visible light and the spectral information of the far-IR light after passing through the polyimide substrate without the sample simultaneously. As a result, the absolute transient absorption spectra of the phonon
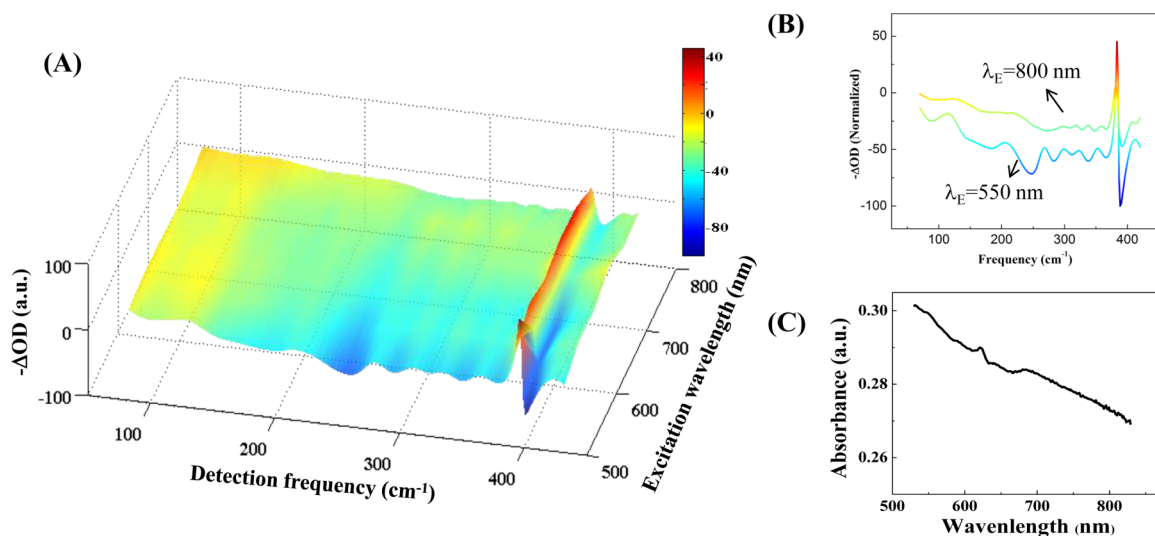
that the heat effect must produce a new absorption at a lower frequency rather than at a higher frequency.

Based on the above analysis, it is very likely that the appearances of the positive peak and the negative peak at 380–390 cm$^{-1}$ are induced by the electron-phonon coupling between the excitations of electrons and the phonon mode $E_{1u}$ of MoS$_2$. This conclusion is further confirmed by the almost identical temporal evolution feature between the signals of these peaks and that of the photo-excited carriers in bulk MoS$_2$ (Fig. 4(d)). The observed relatively higher frequency of the negative peak compared to that of the positive peak



FIG. 7. (a) The two-dimensional visible/far-IR spectrum of bulk MoS$_2$ at waiting time 5 ps. The wavelength of the exciting pulse is scanned from 800 nm to 550 nm. Signal at each exciting wavelength is normalized by the power of the exciting pulse. (b) Comparing the excitation-induced absorption spectral curves in (a) at the excitation wavelength $\lambda_E = 800$ nm and 550 nm (c) The optical absorption spectrum of bulk MoS$_2$.

mode can be accurately extracted. By fitting the perturbed phonon spectra with a proper model, such as Fano lineshape[45] or an asymmetric oscillator,[15] the interactions between the electrons and phonons can be understood.

By scanning the wavelength of the exciting laser pulse from 550 nm to 800 nm, the two-dimensional optical-excitation/far-infrared-detection spectrum of bulk $MoS_2$ is obtained. From the time dependent 2D spectrum, the excitation photon energy dependent (from 2.25 eV to 1.55 eV) charge carrier and electron-phonon coupling dynamics are obtained. Fig. 7(a) displays a 2D spectrum at a waiting time 5 ps, which shows that different excitation frequencies produce very similar responses in the far-IR region. With the decrease of the wavelength of the exciting laser pulse (the increase of the excitation photon energy), the intensities of the signals from both the photo-excited carriers and the electron-phonon coupling increase (see Fig. 7(b)). This is consistent with the optical absorption spectrum of bulk $MoS_2$, i.e., a larger absorbance at a smaller wavelength (see Fig. 7(c)).

## IV. CONCLUDING REMARKS

An ultrafast two-dimensional visible/far-IR spectroscopy based on an optical parametric amplifier and the IR/THz air biased coherent detection method is developed. The method allows the responses in the far-IR region after electronic excitation with tunable excitation frequencies in molecular and material systems to be observed in real time. Using the technique, the photo-excited carriers and electron/phonon coupling dynamics in bulk $MoS_2$ are investigated. It is found that the photo-generation of excited carriers occurs within 160 fs and the relaxation of the carriers is about 30 ps. The electron-phonon coupling between the excitations or motions of electrons and the phonon mode $E_{1u}$ of $MoS_2$ is also directly observed. The coupling shifts the frequency of phonon mode about 9 cm$^{-1}$ higher, resulting in an absorption peak at 391 cm$^{-1}$ and a bleaching peak at 382 cm$^{-1}$. The frequency shift diminishes with the relaxation of the carriers. The dynamics of the electron/phonon coupling resembles that of the photo-excited carriers.

Using the broadband far-IR probe, a very wide variety of molecular and material phenomena can be studied, e.g., charge carrier dynamics in semiconductors, librational modes in water, heat generations induced by electronic motions, charge separations and recombinations, and collective modes in proteins and amino acid crystals. With the tunable excitation wavelengths, one can distinguish the effect of each electronic transition in a system with multiple electronic transitions. Because electron/phonon-vibration couplings are ubiquitous and important in nature, the method demonstrated in this work is expected to be able to gain more applications in other systems, e.g., high-temperature superconductors, nanomaterials, photosynthetic systems, and semiconductors.

[1]J. Bardeen, L. N. Cooper, and J. R. Schrieffer, Phys. Rev. **108**, 1175 (1957).
[2]M. Schluter, M. Lannoo, M. Needels, G. Baraff, and D. Tomanek, Phys. Rev. Lett. **68**, 526 (1992).
[3]Y. Kong, O. Dolgov, O. Jepsen, and O. Andersen, Phys. Rev. B **64**, 020501 (2001).
[4]T. Devereaux, T. Cuk, Z.-X. Shen, and N. Nagaosa, Phys. Rev. Lett. **93**, 117004 (2004).
[5]D. Reznik, L. Pintschovius, M. Ito, S. Iikubo, M. Sato, H. Goka, M. Fujita, K. Yamada, G. Gu, and J. Tranquada, Nature **440**, 1170 (2006).
[6]A. Lanzara, P. Bogdanov, X. Zhou, S. Kellar, D. Feng, E. Lu, T. Yoshida, H. Eisaki, A. Fujimori, and K. Kishio, Nature **412**, 510 (2001).
[7]E. Pop, S. Sinha, and K. E. Goodson, Proc. IEEE **94**, 1587 (2006).
[8]E. Pop, Nano Res. **3**, 147 (2010).
[9]B. Radisavljevic, A. Radenovic, J. Brivio, V. Giacometti, and A. Kis, Nat. Nanotechnol. **6**, 147 (2011).
[10]P. A. George, J. Strait, J. Dawlaty, S. Shivaraman, M. Chandrashekhar, F. Rana, and M. G. Spencer, Nano Lett. **8**, 4248 (2008).
[11]R. Prasankumar, A. Scopatz, D. Hilton, A. Taylor, R. Averitt, J. Zide, and A. Gossard, Appl. Phys. Lett. **86**, 201107 (2005).
[12]H. Němec, F. Kadlec, and P. Kužel, J. Chem. Phys. **117**, 8454 (2002).
[13]A. Nahata, A. S. Weling, and T. F. Heinz, Appl. Phys. Lett. **69**, 2321 (1996).
[14]A. Bingham and D. Grischkowsky, Appl. Phys. Lett. **90**, 091105 (2007).
[15]A. Pashkin, M. Porer, M. Beyer, K. W. Kim, A. Dubroka, C. Bernhard, X. Yao, Y. Dagan, R. Hackl, and A. Erb, Phys. Rev. Lett. **105**, 067001 (2010).
[16]P. Hale, J. Madeo, C. Chin, S. Dhillon, J. Mangeney, J. Tignon, and K. Dani, Opt. Express **22**, 26358 (2014).
[17]M. Yoshizawa and M. Kurosawa, Phys. Rev. A **61**, 013808 (1999).
[18]H. Kuramochi, S. Takeuchi, and T. Tahara, J. Phys. Chem. Lett. **3**, 2025 (2012).
[19]D. W. McCamant, P. Kukura, S. Yoon, and R. A. Mathies, Rev. Sci. Instrum. **75**, 4971 (2004).
[20]S. Laimgruber, W. J. Schreier, T. Schrader, F. Koller, W. Zinth, and P. Gilch, Angew. Chem., Int. Ed. **44**, 7901 (2005).
[21]R. D. Mehlenbacher, B. Lyons, K. C. Wilson, Y. Du, and D. W. McCamant, J. Chem. Phys. **131**, 244512 (2009).
[22]K. E. Dorfman, B. P. Fingerhut, and S. Mukamel, Phys. Chem. Chem. Phys. **15**, 12348 (2013).
[23]B. P. Fingerhut, K. E. Dorfman, and S. Mukamel, J. Chem. Theory Comput. **10**, 1172 (2014).
[24]J. Dai, J. Liu, and X.-C. Zhang, IEEE J. Sel. Top. Quantum Electron. **17**, 183 (2011).
[25]J. Dai, B. Clough, I.-C. Ho, X. Lu, J. Liu, and X.-C. Zhang, IEEE Trans. Terahertz Sci. Technol. **1**, 274 (2011).
[26]X. Sun, F. Buccheri, J. Dai, and X.-C. Zhang, *Photonics Asia* (International Society for Optics and Photonics, 2012), p. 856202.
[27]D. Cook and R. Hochstrasser, Opt. Lett. **25**, 1210 (2000).
[28]M. Kreß, T. Löffler, M. D. Thomson, R. Dörner, H. Gimpel, K. Zrost, T. Ergler, R. Moshammer, U. Morgner, and J. Ullrich, Nat. Phys. **2**, 327 (2006).
[29]M. Kress, T. Löffler, S. Eden, M. Thomson, and H. G. Roskos, Opt. Lett. **29**, 1120 (2004).
[30]X. Xie, J. Dai, and X.-C. Zhang, Phys. Rev. Lett. **96**, 075005 (2006).
[31]H. Chen, H. Bian, J. Li, X. Guo, X. Wen, and J. Zheng, J. Phys. Chem. B **117**, 15614 (2013).
[32]H. Chen, Y. Zhang, J. Li, H. Liu, D.-E. Jiang, and J. Zheng, J. Phys. Chem. A **117**, 8407 (2013).
[33]N. Karpowicz, J. Dai, X. Lu, Y. Chen, M. Yamaguchi, H. Zhao, X.-C. Zhang, L. Zhang, C. Zhang, and M. Price-Gallagher, Appl. Phys. Lett. **92**, 011131 (2008).
[34]X. Lu, N. Karpowicz, and X.-C. Zhang, J. Opt. Soc. Am. B **26**, A66 (2009).
[35]N. Karpowicz, J. Dai, X.-C. Zhang, L. Zhang, and C. Zhang, Int. J. High Speed Electron. Syst. **18**, 1005 (2008).
[36]J. T. Kindt and C. A. Schmuttenmaer, J. Chem. Phys. **110**, 8589 (1999).
[37]P. Kužel, F. Kadlec, and H. Němec, J. Chem. Phys. **127**, 024506 (2007).
[38]S. Kaiser, C. Hunt, D. Nicoletti, W. Hu, I. Gierz, H. Liu, M. Le Tacon, T. Loew, D. Haug, and B. Keimer, Phys. Rev. B **89**, 184516 (2014).
[39]W. Hu, S. Kaiser, D. Nicoletti, C. Hunt, I. Gierz, M. Hoffmann, M. Le Tacon, T. Loew, B. Keimer, and A. Cavalleri, Nat. Mater. **13**, 705 (2014).

[40]T. Wieting and J. Verble, Phys. Rev. B **3**, 4286 (1971).

[41]Y. Cai, J. Lan, G. Zhang, and Y.-W. Zhang, Phys. Rev. B **89**, 035438 (2014).

[42]Q.-C. Sun, X. Xu, L. Vergara, R. Rosentsveig, and J. Musfeldt, Phys. Rev. B **79**, 205405 (2009).

[43]C. Ataca, M. Topsakal, E. Akturk, and S. Ciraci, J. Phys. Chem. C **115**, 16354 (2011).

[44]A. Molina-Sanchez and L. Wirtz, Phys. Rev. B **84**, 155413 (2011).

[45]N. Dean, J. Petersen, D. Fausti, R. a. I. Tobey, S. Kaiser, L. Gasparov, H. Berger, and A. Cavalleri, Phys. Rev. Lett. **106**, 016401 (2011).

[46]C. Lui, A. Frenzel, D. Pilon, Y.-H. Lee, X. Ling, G. Akselrod, J. Kong, and N. Gedik, Phys. Rev. Lett. **113**, 166801 (2014).

[47]H. Chen, H. Bian, J. Li, X. Wen, and J. Zheng, Int. Rev. Phys. Chem. **31**, 469 (2012).

[48]H. Chen, H. Bian, J. Li, X. Wen, and J. Zheng, J. Phys. Chem. A **117**, 6052 (2013).

[49]N. Kumar, J. He, D. He, Y. Wang, and H. Zhao, J. Appl. Phys. **113**, 133702 (2013).

[50]Y.-H. Lee, L. Yu, H. Wang, W. Fang, X. Ling, Y. Shi, C.-T. Lin, J.-K. Huang, M.-T. Chang, and C.-S. Chang, Nano Lett. **13**, 1852 (2013).

[51]See supplementary material at http://dx.doi.org/10.1063/1.4921573 for more figure and texts to further support and explain conclusions in the main text.

Supporting Information

# Electron-Phonon Interactions in MoS$_2$ Probed with Ultrafast Two-Dimensional Visible/Far-Infrared Spectroscopy

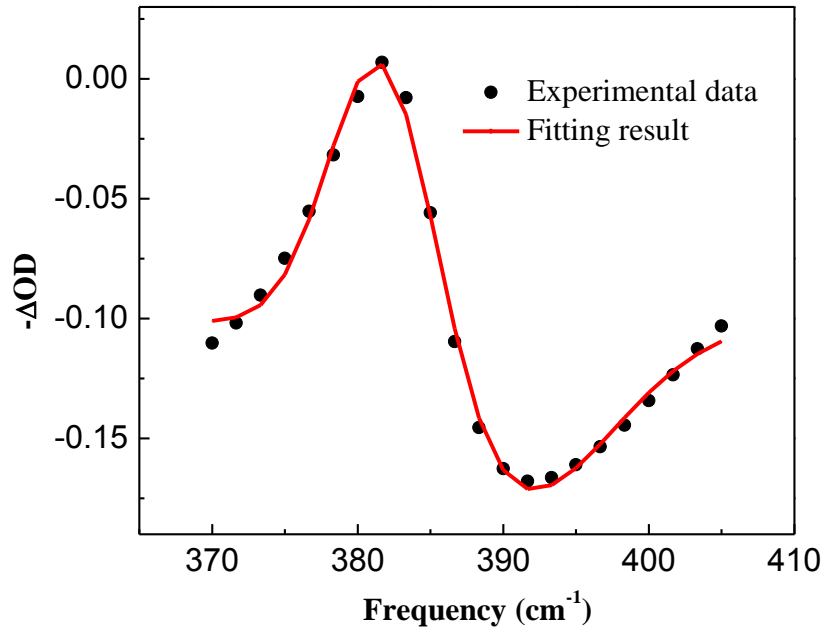*Xunmin Guo[‡], Hailong Chen[‡], Xiewen Wen, and Junrong Zheng\**

**Figure S1.** *Fitting the transient absorption change ($T_W = 2$ ps) of Bulk MoS$_2$ with the superposition of two Gaussian line shapes in the frequency range of phonon mode E$_{1u}$. The dots denote the experimental data, and the solid line denotes Gaussian peak fit. The fitting result shows a sharp positive peak and a negative peak with center frequencies at 382 cm$^{-1}$ and 391 cm$^{-1}$ respectively, indicating the coupling shifts the frequency of phonon mode about 9 cm$^{-1}$ higher. The peak frequencies have an uncertainty of about 2~3 cm$^{-1}$, due to the relatively low signal/noise ratio and the irregular shapes of the samples*

**Estimate MoS₂ temperature jump by excitation**

With the following parameters:

Thermal capacity of bulk $MoS_2$: 63.7 J/(mol·K)

Density: 5.06 g/cm$^3$

Mol mass: 160.07 g/mol

Excitation beam Area: $3.14*0.5^2$ mm$^2$

Coverage of $MoS_2$ on the polyimide substrate: >50%

Thickness of the sample: >0.01mm

Energy absorbed by the sample: <1uJ

The temperature jump can be estimated as:

$$\Delta T_{max} = \frac{1\mu J \cdot 160.07 \frac{g}{mol}}{63.7 \frac{J}{mol \cdot K} \cdot 5.06 \frac{g}{cm^3} \cdot 0.5 \cdot \pi \cdot 0.05^2 \cdot 0.001 cm^3} = 0.13(K)$$
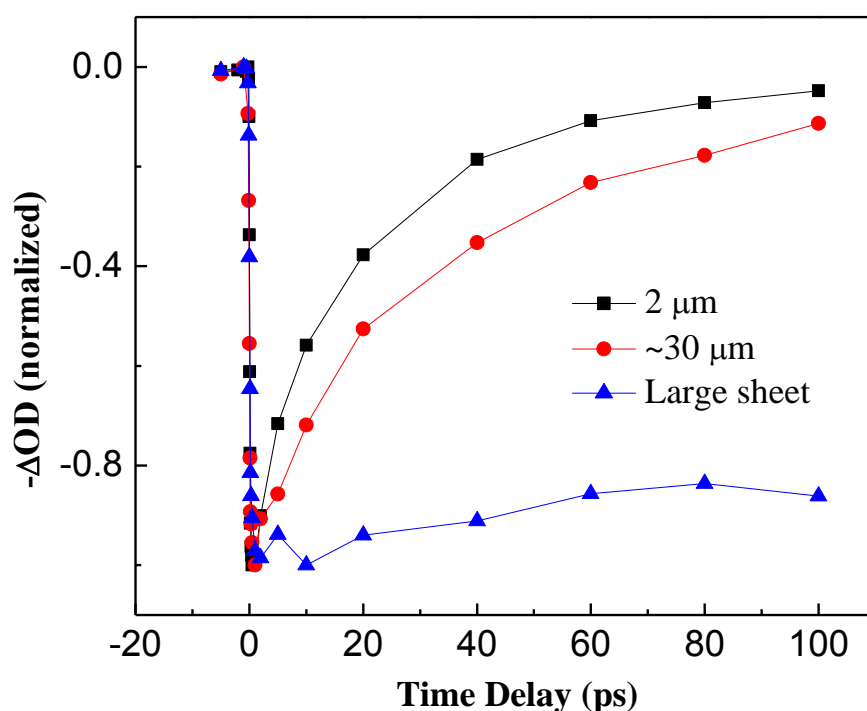
**Figure S2.** *Carrier generation and recombination dynamics of MoS$_2$ samples with different particle sizes detected at 200 cm$^{-1}$ with excitation at 800 nm. The generation dynamics is hardly affected by the sample size. However, the recombination dynamics are dependent on the sample particle size. A sample with larger particles has a slower recombination dynamics. We suspect that there are two possible reasons responsible for the observation: (1) a small particle has more surface defected or trapped states that can facilitate the charge recombination; and (2) a larger particle can have a larger conjugation for carriers to diffuse and make the recombination more difficult, which is probably less likely. The detailed mechanisms for the observed particle size dependent dynamics are subject to future studies. The optical images of the samples are provided in fig.S3.*
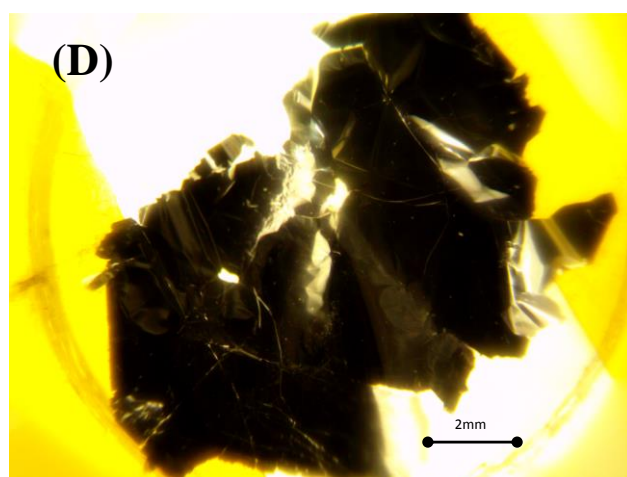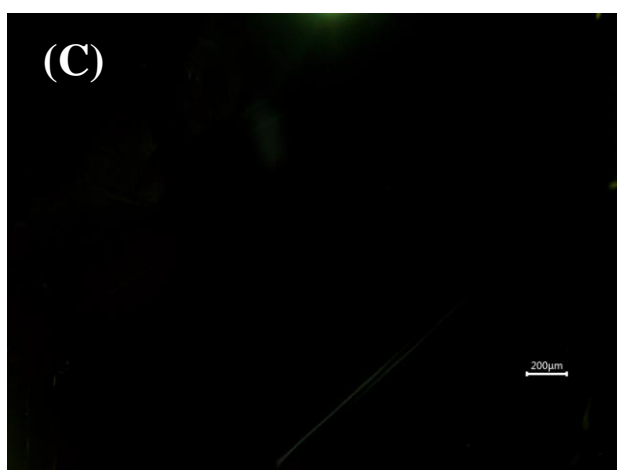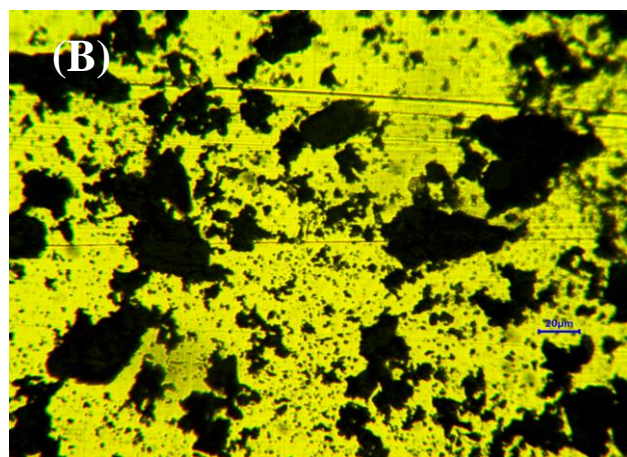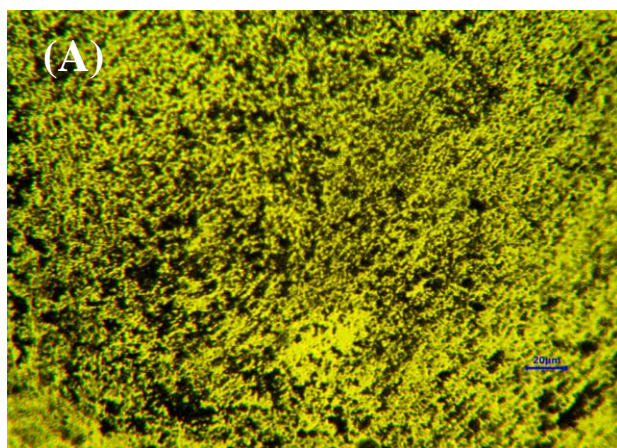
**Figure S3.** *Optical images of samples with length and width of (A) about 2 microns with a thickness of a few microns; (B) about 30 microns with a thickness of a few microns; (C) larger than 1mm; and (D) a zoomed-out image of (C) with a thickness of tens of microns.*
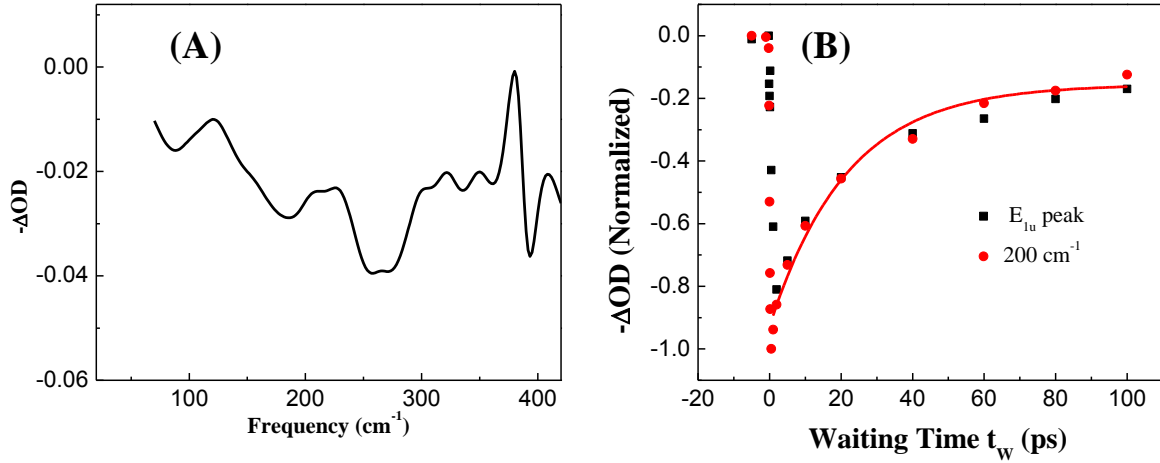
**Figure S4.** *The excitation-induced signal of the bulk MoS$_2$ measured at low excitation power, which is about 35 $\mu J/cm^2$. The wavelength of the exciting pulse is centered at 800 nm. (A) Excitation-induced negative absorption change of bulk MoS$_2$ at the waiting time $T_W$ = 2 ps. Within the experimental error (the signal to noise ratio noise is decreased because of much lower excitation power), the spectral shape is almost the same as that shown in Fig.3B, i.e., among a broadband negative signal, a sharp positive peak at around 380 cm$^{-1}$ and a sharp negative peak at around 390 cm$^{-1}$ appear, indicating the excitation-induced frequency shift of the phonon mode $E_{1u}$. (B) Comparing the normalized waiting time dependent signal from the phonon mode $E_{1u}$ (black dots) with that from photo-excited carriers (measured at 200 cm$^{-1}$, red dots). The red curve is the single exponential fit for the detected signal at 200 cm$^{-1}$ with decay constant 22±3 ps. The result is also similar as that measured at higher excitation power (see Fig.4D), i.e. after the excitation, the intensities of signals from both of the photo-excited carriers and the phonon mode increase rapidly within a couple of hundreds fs and then decay relatively slowly at the time scale of tens of ps, indicating the appearances of the positive peak and the negative peak at 380~390 cm$^{-1}$ are induced by the electron-phonon coupling between the excitations of electrons and the phonon mode $E_{1u}$ of MoS$_2$.*

**Normalization of Excitation-Induced Transient Spectra**

For the spot size of the excitation beam is not large enough to completely cover the entire detection beam, the excitation-induced transient spectra can be approximately normalized in the following manner.

Considering the focal spot diameter of a Gaussian beam is inversely proportional to the frequency of the beam, the spot size of the detection beam on the sample is a function of the frequency ω: $r \propto \omega^{-1}$, where r is the spot radius of the detection beam. For simplicity, the detection beam can be treated as a uniform circular spots with the radius $r$, and the excitation beam is a Gaussian beam, which overlaps with the detection beam on the sample. According to the intensity distribution of the Gaussian beam, we have the average excitation intensity within the area of the detection beam $I(r) \propto [1 - e^{-2r^2/r_0^2}]/r^2$, where $r_0$ is the waist size of the excitation beam. Assuming $r_0$ equal to the spot radius of the detection beam at frequency $\omega_0$, and considering $r \propto \omega^{-1}$, we have $I(\omega) \propto [1 - e^{-2\omega_0^2/\omega^2}] \cdot \omega^2$. Since the signal we measured $-\Delta OD(\omega)$ is proportional to the average intensity of the excitation beam, the excitation-induced transient spectra can be normalized with the coefficient $1/I(\omega)$.

Based on the above analysis, the normalized excitation-induced negative absorption change of MoS$_2$ at a waiting time $T_W$ = 2 ps is calculated (see Fig.S5), where we choose $\omega_0$=250 cm$^{-1}$. Comparing to the unnormalized spectrum, an opposite slope of the transient spectrum is obtained, i.e., increasing absorption with lowering frequencies. For both of the unnormalized and normalized transient spectra, the oscillation background shown in Fig.3B, which arises from the interference introduced by the polyimide substrate, were removed with a cosine function by considering the thickness (~30 μm) and refractive index (~1.7) of the substrate.
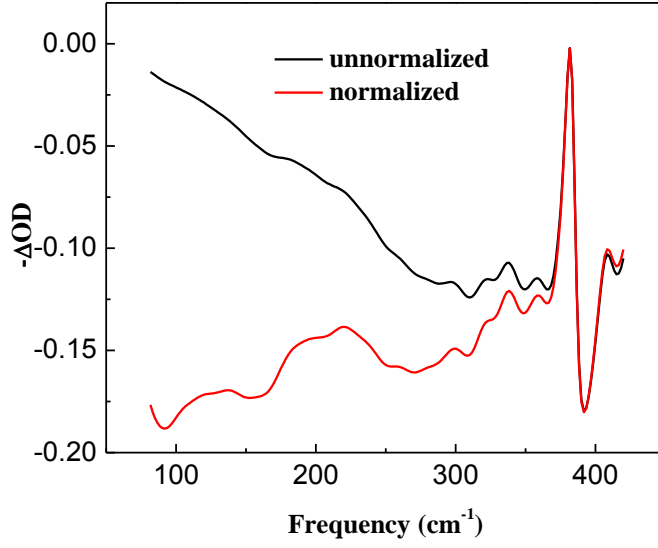
**Figure S5.** *Comparing the unnormalized and normalized excitation-induced negative absorption change of MoS$_2$ at a waiting time $T_W = 2$ ps. The wavelength of the exciting pulse is centered at 800 nm.*

According to eq. 1, we have

$$-\Delta OD(\omega) = \log(\frac{I(\omega)}{I_0(\omega)}) = \log(\frac{|E_0(\omega) + \Delta E(\omega)|^2}{|E_0(\omega)|^2})$$

$$\approx \log(1 + \frac{2\operatorname{Re}\left(E_0(\omega) \cdot \Delta E^*(\omega)\right)}{|E_0(\omega)|^2}) \approx \frac{2\operatorname{Re}\left(E_0(\omega) \cdot \Delta E^*(\omega)\right)}{|E_0(\omega)|^2} \quad . \qquad \text{Eq.S1}$$

According to the literatures[1, 2], we have the differential optical conductivity

$$\Delta \sigma(\omega) \propto -\frac{\Delta E(\omega)}{E_0(\omega)} \quad , \qquad\qquad \text{Eq.S2}$$

with the real part

$$\operatorname{Re}\left(\Delta\sigma(\omega)\right) \propto -\operatorname{Re}\left(\frac{\Delta E(\omega)}{E_0(\omega)}\right)$$

$$= -\operatorname{Re}\left(\frac{\Delta E(\omega) \cdot E_0^*(\omega)}{|E_0(\omega)|^2}\right) = -\frac{\operatorname{Re}\left(E_0(\omega) \cdot \Delta E^*(\omega)\right)}{|E_0(\omega)|^2} \quad . \qquad \text{Eq.S3}$$

$$\propto \Delta OD(\omega)$$

It means the real part of the photo-induced increase of THz conductivity in MoS$_2$ samples has the

same line shape as the normalized excitation-induced negative absorption change shown in fig.S5, and therefore, can be described roughly by the Drude formula.[1]

However, it does not mean the optical excitation enhanced absorption signal we measured is from the free carrier Drude response. The above method of normalization is just a rough estimate. In the calculations, we assumed the detection beam on the sample is a uniform circular spot. However, the real situation is that, the intensity distribution of the detection beam generated by THz-ABCD method can be very complicate and hard to predict. In addition, we also assumed that the waist size of the excitation beam $r_0$ is equal to the spot radius of the detection beam at frequency $\omega_0 = 250$ cm$^{-1}$, which may not be accurate either. If we choose $\omega_0 = 100$ cm$^{-1}$, the same slope of the transient spectrum as the unnormalized one will be obtained, and then the localization rather than a free carrier response may explain our experimental results better.

[1] C. Lui, A. Frenzel, D. Pilon, Y.-H. Lee, X. Ling, G. Akselrod, J. Kong, and N. Gedik, Phys. Rev. Lett. **113**, 166801 (2014).
[2] G. Jnawali, Y. Rao, H. Yan, and T. F. Heinz, Nano lett. **13**, 524 (2013).